Proceedings of the 2010 IEEE
International Conference on Mechatronics and Automation
August 4-7, 2010, Xi'an, China

A Novel Approach of Initializing Region-Based Active Contours in Noisy Images by Means of Higher Order Statistics and Dissimilarity

Kevin Ohliger, Torsten Edeler, Stephan Hussmann, Alexandru Paul Condurache, and Alfred Mertins, Senior Member, IEEE

Abstract— **In this paper we present two novel methods for initializing region-based active contours. First we use an analysis of higher order statistic attributes of the complete image and the regions of the initial contour candidates. Then we extend this approach by taking the dissimilarity between the initialized regions and the complete image into account. We compare our method with the standard initialization of active contours for different types and degree of noise in synthetic and real images. It is shown that our method outperforms state of the art initializations of active contours considering the total accuracy and Cohen's kappa.**

Index Terms - **active contours, initialisation, noise, kurtosis, dissimilarity, Cohen's kappa, overall accuracy, KR, KDR, higher order statistics, HOS**

I. INTRODUCTION

As an important part of image processing segmentation of a scene is still a challenging task and is topic of current research. In 1988 Kass et al. [1] introduced a new segmentation method based on active contour models, also called snakes, using local edge information. An active contour model includes an external energy term which is driven by image data and an internal energy term which makes the active contour behave like an elastic material. Active contours Using edge detectors for the external force were successfully applied for different segmentation applications in [2], [3], [4], [5]. The problems caused by the edge detectors are their sensitivity to noise and discontinuous boundaries in the image as shown in [6]. They were first substituted by region-based approaches in [7]. Related to the Mumford-Shah functional Chan and Vese [6] developed a model assuming that an image is piecewise constant including level sets allowing topological changes of the contours introduced by Osher and Sethian [8]. Shi and Karl [9] introduced a fast level set algorithm without solving partial differential equations.

Kevin Ohliger, Torsten Edeler, and Stephan Hussmann are with the Institute for Machine Vision Technology (Ma.Vi.Tec), Westcoast University Heide, 25746 Heide, Germany ohliger@fh-westkueste.de

Alexandru Paul Condurache, and Alfred Mertins are with the Institute for Signal Processing, University of Lübeck, D-23538 Lübeck, Germany.

In [10], [11], [12], [13] geodesic active contour algorithms were developed, for which the initialization step is not crucial. Nevertheless most active contour algorithms need an appropriate initialization of the starting contours. These contours have significant influence on the segmentation result as it is shown in this work. The different initializations may result in a local minimum of the functional energy of the active contours and not in the desired global minimum. Bresson et al. [14] introduced a fast global minimization of the active contour model which is based on the combination of segmentation and denoising without depending on initial contour positions.

There exist only a few initialization methods in literature up to now. The easiest and probably best initialization is done manually by the user as described in [15], [16], [17], [18]. Another common method for initializing the active contours are seed contours placed in a regular grid in the image [15], [19], [20] while no adaption of the grid pitch or initial contour size to image data are made. Our approach is to adapt the radii of the initial contours placed on a regular grid by means of analysis of the local and global image data.

The outline of the paper is as follows. In Section II we introduce our active contour model and in Section III our image model. In the following section we derive our two approaches for adaption of the initial contours. We show in Section V experimental results on synthetic and real images and finally conclude and give an outlook in Section VI.

II. ACTIVE CONTOUR MODEL

The energy of a classical active contour (AC) model E_{AC} (see [1]) includes an internal energy E_{int} and an external energy E_{ext}

$$E_{\mathrm{AC}}(u, C) = E_{\mathrm{int}}(C) + E_{\mathrm{ext}}(u, C) \quad . \tag{1}$$

E_{int} depends on the contour C only and forces the contour to become smooth and E_{ext} includes the influence

[0]This project is sponsored by the European Union (EFRE) and the federal state of Schleswig-Holstein, Germany (Zukunftsprogramm Wirtschaft)

ZUKUNFTSprogramm
Wirtschaft
Investition in Ihre Zukunft

of the function u describing the image. We use a region-based active contour model introduced by [7] defining the energy of a single contour i

$$E_{\mathrm{AC},i}\left(u, C_i, \theta_{\mathbf{i}}\right) = \frac{\mu}{2}\mathrm{Length}\left(C_i\right) - \iint_{(x,y)\in R_i} \ln P\left(u\left(x,y\right) \mid \theta_{\mathbf{i}}\right)\, dx\, dy. \quad (2)$$

R_i is the region enclosed by contour C_i and $\theta_{\mathbf{i}}$ contains the statistical parameters describing a feature probability density function of R_i. $\mathrm{Length}(C_i)$ is the length of the boundary curve and μ a positive weighting factor for the smoothness term. The segmentation result is achieved when the energy of the contour set C including P contours C_i is minimal

$$\tilde{\mathbf{C}} = \arg\min_{C_i\in C} \sum_{i=1}^{P} \left[E_{\mathrm{AC}}\left(u, C_i, \theta_{\mathbf{i}}\right) + \lambda\right] \quad (3)$$

$$= \arg\min_{C_i\in C} \sum_{i=1}^{P} \left[\frac{\mu}{2}\mathrm{Length}\left(C_i\right) \quad (4) \right.$$

$$\left. - \iint_{(x,y)\in R_i} \ln P\left(u\left(x,y\right) \mid \theta_{\mathbf{i}}\right)\, dx\, dy + \lambda\right]. \quad (5)$$

λ is a positive constant for avoiding oversegmentation and $\tilde{\mathbf{C}}$ is the set of final contours.

The parameters $\theta_{\mathbf{i}}$ are estimated based on the sampled image data matrix $\mathbf{U_0}$ with dimension K x L. We assume that $\mathbf{U_0}$ contains M different objects ω_j with a feature (e.g. intensity values) that can be described by a unimodal Gaussian distribution $\mathcal{N}\left(\mu_{\omega_j}, \sigma^2_{\omega_j}\right)$. μ_{ω_j} and $\sigma^2_{\omega_j}$ are the feature mean and variance of the respective object. The parameters

$$\theta_i = [\theta_{i,0}, \theta_{i,1}] = [\mu_{R_i}, \sigma^2_{R_i}] \quad (6)$$

of a unimodal Gaussian distribution $\mathcal{N}\left(\theta_{i,0}, \theta_{i,1}\right)$ for Region R_i are estimated by

$$\theta_{i,0} = \sum_{j=1}^{M} \alpha_{j,i} \cdot \mu_{\omega_j} \quad , \quad (7)$$

and

$$\theta_{i,1} \approx \frac{N_{R_i}}{N_{R_i}-1} \sum_{j=1}^{M} \alpha_{j,i} \left[\sigma^2_{\omega_j} + \left(\mu_{R_i} - \mu_{\omega_j}\right)^2\right] \quad , \quad (8)$$

while $\alpha_{j,i}$ describes the ratio of ω_j outcomes in region R_i to complete count of outcomes N_{R_i} of R_i. The approximated variance (8) leads to good results for N_{R_i} >100.

III. Image Model

In this section we introduce the image model used. As mentioned in Section II the undistorted image data $\mathbf{U_0}$ is assumed to include $M \in [2, K\cdot L]$ different objects

$$u_0\left(k,l\right) = \sum_{j=1}^{M} f_{\omega_j}\left(k,l\right) \quad , \quad (9)$$

with $k = 1,\ldots,K$, $l = 1,\ldots,L$, and

$$f_{\omega_j}\left(k,l\right) = \begin{cases} F_j\left(k,l\right) & k,l \text{ inside of } \omega_j \\ 0 & \text{otherwise} \end{cases} . \quad (10)$$

$\mathbf{F}_j$ is described by

$$\mathbf{F}_j \sim \mathcal{N}\left(\mu_{\omega_j}, \sigma^2_{\omega_j}\right) \quad . \quad (11)$$

We extend our model (9) with additive noise $\mathbf{N}$ resulting in the noisy image

$$\mathbf{U} = \mathbf{U_0} + \mathbf{N} \quad , \quad (12)$$

while $\mathbf{N}$ is independent identically distributed noise. We concentrate on additive white Gaussian noise with zero mean and variance σ^2_n

$$\mathbf{N_g} \sim \mathcal{N}\left(0, \sigma^2_n\right) \quad (13)$$

and uniformly distributed noise

$$\mathbf{N_u} \sim \mathcal{U}\left(0, W\right) \quad , \quad (14)$$

with $\mathcal{U}$ described by the probability density function (pdf)

$$p_{\mathcal{U}}\left(v\right) = \begin{cases} 1/W & -W/2 \le v \le W/2 \\ 0 & \text{otherwise} \end{cases} . \quad (15)$$

W is the width of the uniform distribution.

IV. Adaption of the Initial Contour

This section describes our approach for adaption of the initial contour based on higher order statistics. It is obvious that (5) is strongly influenced by the estimated parameters θ_i. Initial contours containing more than one object lead to skewed parameters as expressed in (7) and (8) even in a non distorted image $\mathbf{U_0}$. The general sequence of an automatic selection of regions and their radii based on our two different methods are introduced in the following sections.

A. Initial Contour Adaption Algorithm

We place the center of the region candidates R_i for initial contours in a regular grid with pitch d_0. The initial radii are selected to be maximal without generating overlapping regions, $r_0 = d_0/2$. The radius for each region is iteratively decreased until the region is expected to include a single object. According to our image model (12) the contained pdf in this case is a unimodal Gaussian pdf distorted by an additive noise. R_i is a valid initial contour if this is achieved. If a radius is decreased to a fixed minimum $r_{\min}$, while containing two or more objects, the region is ignored. In Section IV-B and IV-C two methods for analyzing the pdf with respect to the included object count are derived.

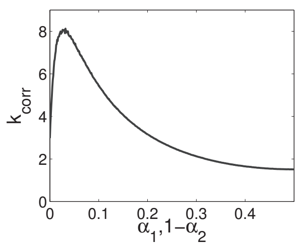

Fig. 1. Simulated bias corrected kurtosis k_{corr} dependent on the bimodal mixture described by the weighting coefficients α_1 and α_2 of the distributions $\mathcal{N}_1(0.25, 0.1)$ and $\mathcal{N}_2(0.75, 0.1)$.The simulation was done on 20000 samples.

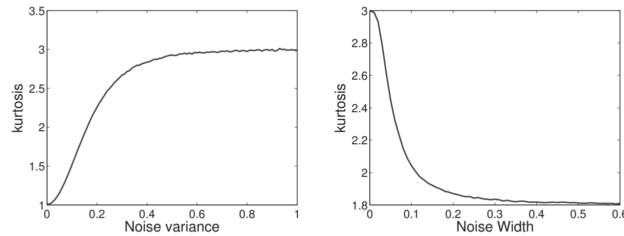

(a) (b)

Fig. 2. Simulated bias corrected kurtosis k_{corr} dependent on additive Gaussian noise on a region with bimodal Gaussian distribution $\alpha_1 = \alpha_2$ of the distributions $\mathcal{N}_1(0.25, 0.1)$ and $\mathcal{N}_2(0.75, 0.1)$ (a) and k_{corr} dependent on uniformly distributed noise on a region with unimodal Gaussian distribution $\mathcal{N}_3(0.5, 0.1)$. The simulation was done on 20000 samples.

B. Kurtosis Driven Radius (KR)

If two or more unimodal Gaussian distributions $\mathcal{N}_1, \ldots, \mathcal{N}_K$ are overlapping inside one region the type of the mixed distribution $\mathcal{M}$ depends on the parameters of the single distributions. If at least one mean value differs from the other mean values, $\mathcal{M}$ will be a multimodal Gaussian distribution. Inspired by [21], [22], [23] we choose the kurtosis using the bias corrected formula

$$k_{\mathrm{corr}}(\mathbf{x}) = \frac{L-1}{(L-2)(L-3)}\left[(L+1)\,k(\mathbf{x}) - 3(L-1)\right] + 3 \quad (16)$$

with

$$k(\mathbf{x}) = \frac{\sum_{i=1}^{L}(x_i-\mu)^4}{\frac{1}{L}\left[\sum_{i=1}^{L}(x_i-\mu)^2\right]^2} \quad (17)$$

as an indicator of multimodal Gaussian distributions with L samples x_i. As shown in Fig. 1 the kurtosis for a unimodal Gaussian distribution ($\alpha_1 = 0$) is approximately three. For $\alpha_1 \approx 0.2$ indicating that 20 percent of the region is filled with another object the kurtosis is also three. This will lead to initial contours with a multi object region. Depending on the global image noise determined by the kurtosis of the image $k_{\mathrm{corr}}(\mathbf{U})$ a threshold T_k with negative correlation to k_{corr} is chosen based on the simulation results shown in Fig. 1 as a limit for the acceptable kurtosis for an initial contour region. The decision if the region R_i is a valid initial contour is based on the condition

$$\left|k_{\mathrm{corr}}(u((x,y) \in R_i)) - 3\right| \leq T_k \ , \quad (18)$$

while $|:|$ denotes the respective absolute value.

C. Kurtosis and Dissimilarity Driven Radius (KDR)

One main problem of the method introduced in IV-B is the noise sensitivity of the kurtosis as shown in Fig. 2 for Gaussian noise (a) and uniformly distributed noise (b). It is shown that the kurtosis of an image is positive correlated to the additive Gaussian noise energy and negative correlated to the uniformly distributed noise energy. Gaussian noise will lead to initial contours containing invalid regions and uniformly distributed noise will lead to refusing of valid regions. To overcome this we introduce a dissimilarity measure which contains the Wasserstein metric [24] between the estimated cumulated probability density function (cdf) F of the local region R_i and the global image $\mathbf{U}$

$$d_{\mathcal{W}}(F_{R_i}, F_u) \quad = \quad \int_{-\infty}^{\infty}\left|F_{R_i}(v) - F_u(v)\right| dv \ . \quad (19)$$

The selection of the threshold for the dissimilarity T_d with positive correlation to k_{corr} is based on the simulation results shown in Fig. 2 (a) and (b). The condition

$$d_{\mathcal{W}}(F_{R_i}, F_u) > T_d \quad (20)$$

refuses regions with cdfs which are too similar to the global image cdf and hence are dominated by the noise. A disadvantage that arises is that the dissimilarity depends on the mean value of R_i. Regions with mean values similar to the mean value of $\mathbf{U}$ tend to be rejected. The conditions (18) and (20) are combined for the KDR method.

V. Experimental Results

For evaluation of the methods for contour initializing, the segmentation results for a synthetic image fulfilling our image model (12) and for two real images are compared. The accuracy of the labeled segmentation image $\tilde{\mathbf{L}}$ was measured by the overall accuracy (OA)

$$OA\left(\tilde{\mathbf{L}}, \mathbf{L}\right) = \sum_{i=1}^{M}\frac{\max\left(A\left(\tilde{\mathbf{L}} \cap \mathbf{L_i}\right)\right)}{A(\mathbf{L_i})} \ , \quad (21)$$

while every labeled region in $\tilde{\mathbf{L}}$ is considered once and $\max(:)$ returns the maximum value. $A(:)$ is the area of the respective region. $\mathbf{L}$ is the labeled reference containing M single segmentation labels $\mathbf{L_i}$. In addition to OA, Cohen's kappa is used

$$\kappa = \frac{p_o - p_c}{1 - p_c} \ , \quad (22)$$

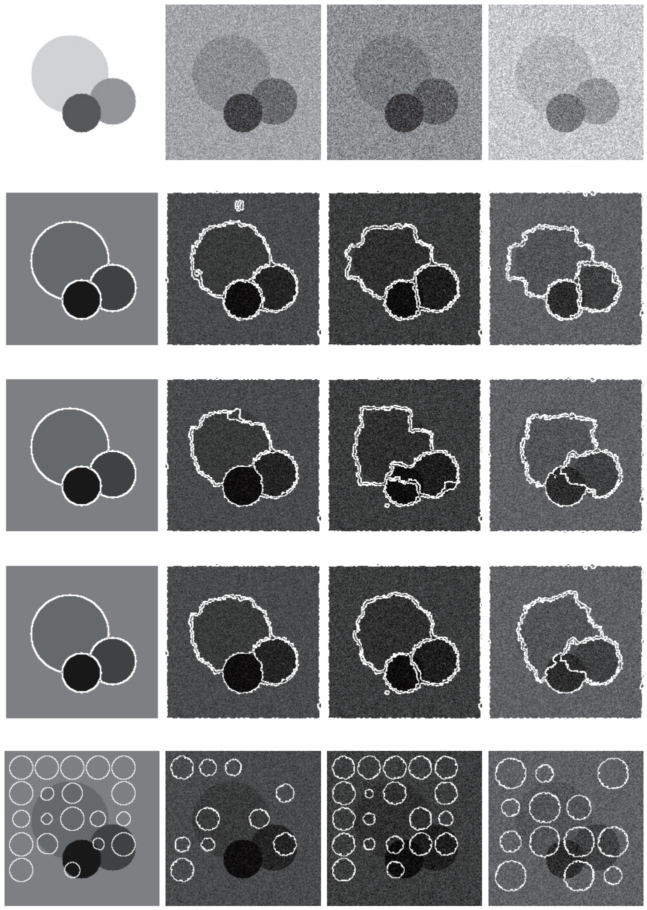

(a) (b) (c) (d)

Fig. 3. Row 1: Scaled synthetic image to [0,1] with Gaussian noise σ_n^2 = 1e-8 (a), σ_n^2 = 4e-2 (b), σ_n^2 = 9e-2 (c), and uniformly distributed noise W = 1 (d). Row 2: Segmentation result for best fixed radius: r = 10 (a), r = 5 (b), r = 10 (c), and r = 10 (d). Row 3: Segmentation result KR method. Row 4: Segmentation result for KDR method. Row 5: Initial contours of KDR method. For Row 2 to 5 the images are scaled to [0,0.8] in order to emphasize the contour lines.

where p_o is the proportion of units in which agreement is reached and p_c is the proportion of units for which agreement is expected by chance (more details are given in [25]).

The parameter of the active contours energy (5) including λ and μ are fixed for each configuration of the input image in order to provide comparability of the segmentation results. Between the different images and different noise levels the parameters are configured to provide accurate results. The experimental results are focussing on the dependency of the active contour algorithm on the initial contours and not on the optimal parameter for energy minimization of the active contours.

A. Synthetic Image

The synthetic image generated for evaluation of the different methods contains three overlapping circular

TABLE I

Segmentation Accuracy for the Synthetic Image with Additive Gaussian Noise

Type	σ_n^2,W	Method	OA	κ
Gaussian	1e-8	Fixed Radius 20	0.9949	0.9885
		Fixed Radius 10	**0.9995**	**0.9989**
		Fixed Radius 5	0.9994	0.9988
		KR	**0.9995**	**0.9989**
		KDR	**0.9995**	**0.9989**
Gaussian	4e-2	Fixed Radius 20	0.9399	0.8666
		Fixed Radius 10	0.9803	0.9564
		Fixed Radius 5	**0.9830**	**0.9625**
		KR	0.9700	0.9336
		KDR	0.9804	0.9566
Gaussian	9e-2	Fixed Radius 20	0.9471	0.8827
		Fixed Radius 10	0.9637	0.9198
		Fixed Radius 5	0.9592	0.9106
		KR	0.9393	0.8659
		KDR	**0.9721**	**0.9383**
Uniform	1	Fixed Radius 20	0.8228	0.6075
		Fixed Radius 10	**0.9538**	**0.8980**
		Fixed Radius 5	0.9285	0.8421
		KR	0.9285	0.8421
		KDR	0.9356	0.8580

objects ω_1, ω_2, ω_3, and a background ω_{bg} with the respective means μ_{bg} = 1, μ_1 = 0.2, μ_1 = 0.5, and μ_3 = 0.8. This basic image is distorted by three Gaussian distributed noises $\mathbf{N_1}, \ldots, \mathbf{N_3}$ with $\sigma_{n,1}^2$ = 1e-8, $\sigma_{n,2}^2$ = 4e-2, $\sigma_{n,3}^2$ = 9e-2, and additionally with an uniformly distributed noise $\mathbf{N_4}$ with $W = 1$ resulting in images $\mathbf{U_1}, \ldots, \mathbf{U_4}$. We set for KR and KDR methods the parameters $d_0 = 40$ and $r_{\min} = 5$. For the other methods the maximum pitch was $d_0 = 2r$.

Fig. 3 shows the segmentation results and TABLE I the accuracy measurements. The KDR method leads to best result for $\mathbf{U_1}$ and $\mathbf{U_3}$. In case of $\mathbf{U_2}$ the fixed radius selection $r = 5$ performs best with small difference to the KDR method. Choosing $r = 10$ for $\mathbf{U_4}$ outperforms the other ones. As shown in the fifth row and column (d) of Fig. 3 the KDR method places initial contours on the border of ω_1 which results in a bad segmentation for this region and leading to lower OA and κ.

B. Real Images

The evaluation of the segmentation results for real images was made on two different images of the Berkeley segmentation dataset[1]. The two images shown in Fig. 4 and 5 were chosen. They are expected to be approximately compatible to the image model (12). The segmentation reference $\mathbf{L}$ was also available in the dataset. We choose for KR and KDR methods the parameters d_0 = 30 and $r_{\min}$ = 10. For the other methods the maximum pitch was chosen $d_0 = 2r$.

The results of the segmentation methods for Gaussian noise with σ_n^2 = 1e-8 show small differences in the contour images and also in the OA and κ listed in TABLE II. As it can be seen in column (b), (c) of

[1] http://www.eecs.berkeley.edu/Research/Projects/CS/vision/bsds/

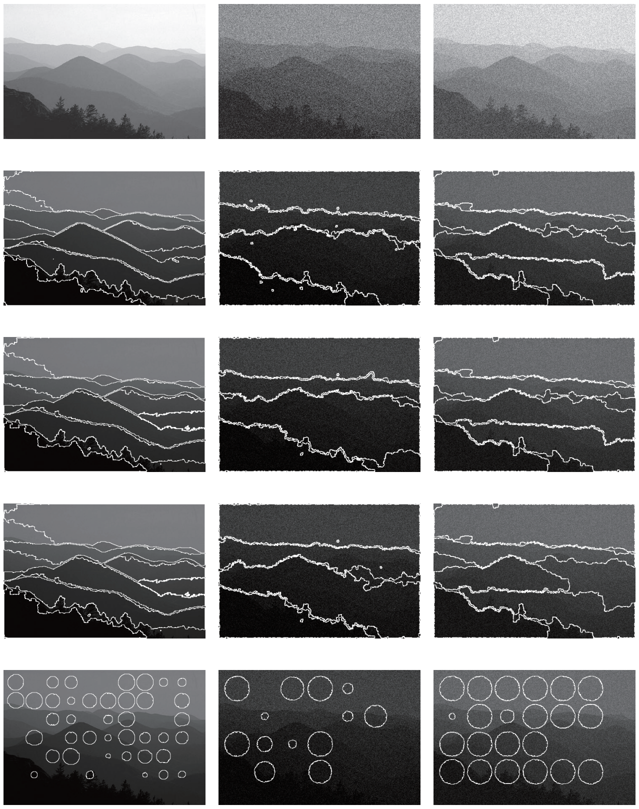

(a) (b) (c)

Fig. 4. Row 1: Scaled real image 1 to [0,1] with Gaussian noise σ_n^2 = 1e-8 (a), σ_n^2 = 4e-2 (b), and uniformly distributed noise with $W = 0.4$ (c). Row 2: Segmentation result for best fixed radius $r = 30$ (a-c). Row 3: Segmentation result for KR method. Row 4: Segmentation result for KDR method. Row 5: Initial contours of KDR method. For Row 2 to 5 the images are scaled to [0,0.8] in order to emphasize the contour lines.

TABLE II
SEGMENTATION ACCURACY FOR REAL IMAGES WITH ADDITIVE GAUSSIAN OR UNIFORM NOISE

Img.	Type	σ_n^2,W	Method	OA	κ
1	Gaussian	1e-8	Fixed Radius 30	**0.9282**	**0.9127**
			Fixed Radius 20	0.9184	0.9009
			Fixed Radius 10	0.8347	0.7990
			KR	0.9245	0.9083
			KDR	0.9245	0.9083
1	Gaussian	4e-2	Fixed Radius 30	0.7110	0.6481
			Fixed Radius 20	0.7088	0.6453
			Fixed Radius 10	0.5662	0.4730
			KR	0.7088	0.6454
			KDR	**0.7221**	**0.6614**
1	Uniform	0.4	Fixed Radius 30	0.8060	0.7638
			Fixed Radius 20	0.7280	0.6688
			Fixed Radius 10	0.7228	0.6622
			KR	0.8060	0.7638
			KDR	**0.8409**	**0,8063**
2	Gaussian	1e-8	Fixed Radius 30	0.7473	0.7079
			Fixed Radius 20	0.7423	0.7022
			Fixed Radius 10	0.6962	0.6489
			KR	**0.8257**	**0.7986**
			KDR	**0.8257**	**0.7986**
2	Gaussian	4e-2	Fixed Radius 30	0.6519	0.5967
			Fixed Radius 20	0.6967	0.6488
			Fixed Radius 10	**0.7128**	**0.6671**
			KR	0.7047	0.6581
			KDR	0.7035	0.6568
2	Uniform	0.4	Fixed Radius 30	0.6283	0.5694
			Fixed Radius 20	0.6444	0.5882
			Fixed Radius 10	0.6990	0.6513
			KR	0.6283	0.5694
			KDR	**0.7138**	**0.6685**

Fig. 4 and Fig. 5, and in TABLE II the segmentation result of KDR for Gaussian noise with high variance σ_n^2 = 4e-2 in image 1 and for uniformly distributed noise with $W = 0.4$ for both images outperforms the other methods. For image 2 with σ_n^2 = 4e-2 the fixed radius with $r = 10$ initialization lead to best result with small difference to the KR and KDR methods. The reason for this was the pitch of the regular grid for the KDR and KR method. The initial contours of KDR method are shown in the last row of Fig. 4 and Fig. 5 with different radii but also refused regions (empty regions in the regular grid).

VI. CONCLUSIONS AND FUTURE WORKS

A. Conclusions

We have developed two novel methods for shaping initial contours based on higher order statistics and a dissimilarity measure. The KR method varies the radii of possible initial contours by interpreting the kurtosis of the enclosed region and of the complete image. The KDR method extends KR by adding a dissimilarity measure based on the cumulative density functions of local and global regions. The methods were evaluated against standard selections of initial contours including different pitches and radii. The automatic radius adaption of the KDR method lead to better or similar results for low noise energy of Gaussian noise for the synthetic and two real images in terms of overall accuracy and Cohen's kappa. For uniformly distributed noise the KDR method outperforms the other methods for real images.

B. Future Works

For the KR and KDR method the kurtosis was used as multimodality measure of distributions. The main focus of our actual research is the investigation of further multimodality measures in order to reduce the noise dependency of active contours initialisation methods.

REFERENCES

[1] M. Kass, A. Witkins, and D. Terzopoulus, "Snakes: active contour models," *International Journal of Computer Vision*, vol. 1, no. 4, 1988.

[2] L. Cohen, "On active contour models and balloons," *CVGIP. Image understanding*, vol. 53, no. 2, pp. 211–218, 1991.

[3] I. Carlbom, D. Terzopoulos, and K. Harris, "Computerassisted registration, segmentation, and 3d reconstruction from images of neuronal tissue sections," *IEEE Trans. Med. Imag.*, vol. 13, no. 2, pp. 351–362, 1994.

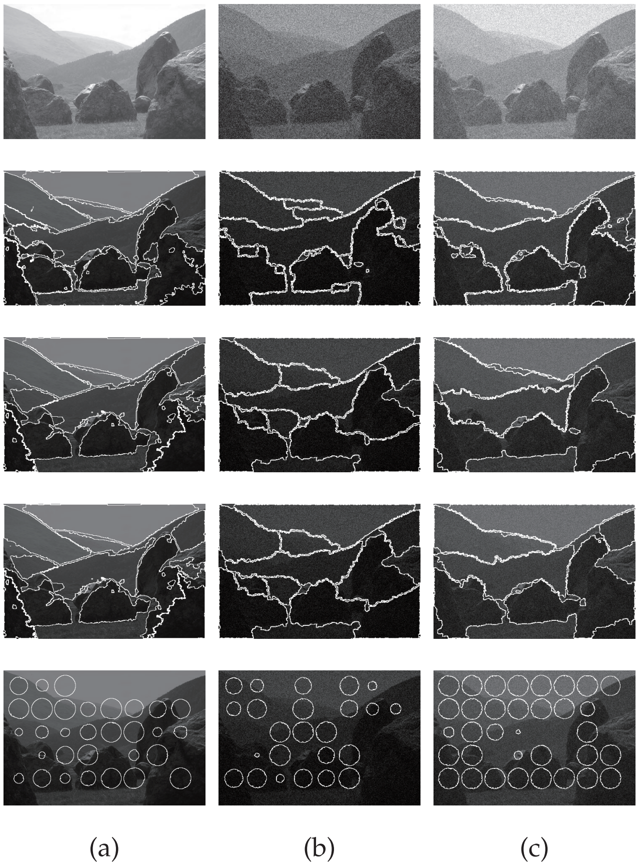

Fig. 5. Row 1: Scaled real image 2 to [0,1] with Gaussian noise σ_n^2 = 1e-8 (a), σ_n^2 = 4e-2 (b), and uniformly distributed noise with $W = 0.4$ (c). Row 2: Segmentation result for best fixed radius $r = 30$. Row 3: Segmentation result for KR method. Row 4: Segmentation result for KDR method. Row 5: Initial contours of KDR method. For Row 2 to 5 the images are scaled to [0,0.8] in order to emphasize the contour lines.

[4] F. Leymarie and M. Levine, "Simulating the grassfire transform using an active contour model," *IEEE Trans. Pattern Anal. Mach. Intell.*, vol. 14, no. 1, pp. 158–175, 1995.

[5] R. Malladi and J. Sethian, "A real-time algorithm for medical shape recovery," *IEEE Trans. Pattern Anal. Mach. Intell.*, vol. 14, no. 1, pp. 158–175, 1995.

[6] T. Chan and L. Vese, "Active contours without edges," *IEEE Trans. Image Process.*, vol. 10, no. 2, pp. 266–277, 2001.

[7] S. Zhu and A. Yuille, "Region competition: unifying snakes, region growing, and bayes/mdl for multiband image segmentation," *IEEE Trans. Pattern Anal. Mach. Intell.*, vol. 18, no. 9, pp. 884–900, 1996.

[8] S. Osher and J. Sethian, "Fronts propagating with curvature-dependent speed: algorithms based on hamilton-jacobi formulations," *Journal of computational physics*, vol. 79, no. 1, pp. 12–49, 1988.

[9] Y. Shi and W. Karl, "A fast level set method without solving pdes," in *IEEE International Conference on Acoustics, Speech, and Signal Processing*, vol. 2, 2000, pp. 304–310.

[10] V. Caselles, R. Kimmel, and G. Sapiro, "Geodesic active contours," in *Fifth International Conference on Computer Vision, 1995. Proceedings.*, 1995, pp. 694–699.

[11] S. Kichenassamy, A. Kumar, P. Olver, A. Tannenbaum, and A. Yezzi, "Gradient flows and geometric active contour models," in *Fifth International Conference on Computer Vision, 1995. Proceedings.*, 1995, pp. 810–815.

[12] R. Malladi, J. Sethian, and B. Vemuri, "Shape modeling with front propagation: a level set approach," *IEEE Trans. Pattern Anal. Mach. Intell.*, vol. 17, no. 2, 2002.

[13] N. Paragios and R. Deriche, "Geodesic active regions for supervised texture segmentation," in *The Proceedings of the Seventh IEEE International Conference on Computer Vision*, vol. 2.

[14] X. Bresson, S. Esedoglu, P. Vandergheynst, J. Thiran, and S. Osher, "Fast global minimization of the active contour/snake model," *Journal of Mathematical Imaging and Vision*, vol. 28, no. 2, pp. 151–167, 2007.

[15] T. McInerney and D. Terzopoulus, "Topologically adaptable snakes," in *IEEE Fifth Int. Conf. on Computer Vision*, 1995.

[16] A. Tsai, A. Yezzi, and A. Willsky, "Curve evolution implementation of the mumford-shah functional for image segmentation, denoising, inerpolation and magnification," *IEEE Trans. Image Process.*, vol. 10, no. 8, pp. 1169–1186, 2001.

[17] G. Tsechpenakis and D. Metaxas, "Crf-driven implicit deformable model," in *IEEE Conference on Computer Vision and Pattern Recognition*, 2007, pp. 1–8.

[18] H. Li and L. Cohen, "3d brain segmentation using dual-front active contours with optional user interaction," *International Journal of Biomedical Imaging*, vol. 2006, 2006.

[19] J. A. Yezzi, A. Tsai, and A. Willsky, "A statistical approach to snakes for bimodal and trimodal imagery," in *The Proceedings of the Seventh IEEE International Conference on Computer Vision, 1999*, vol. 2, 1999.

[20] P. Martin, P. Réfreégier, F. Goudail, and F. Guérault, "Influence of the noise model on level set active contour segmentation," *IEEE Trans. Pattern Anal. Mach. Intell.*, vol. 26, no. 6, 2004.

[21] T. Rao and W. Wong, "Tests for gaussianity and linearity of multivariate stationary time series," *Journal of Statistical Planning and Inference*, vol. 68, pp. 373–386, 1998.

[22] M. Hinich, "Testing for gaussianity and linearity of a stationary time series," *Journal of Time Series Analysis*, vol. 3, no. 3, pp. 169–176, 1982.

[23] R. Darlington, "Is kurtosis really 'peakedness?'," *The American Statistician*, vol. 24, no. 2, pp. 19–22, 1970.

[24] A. Gibbs and F. Su, "On choosing and bounding probability metrics," *Inernational Statistic Review/Revue Internationale de Statistique*, vol. 70, no. 3, pp. 419–435, 2002.

[25] J. Cohen *et al.*, "A coefficient of agreement for nominal scales," *Educational and psychological measurement*, vol. 20, no. 1, pp. 37–46, 1960.